Coupled Computation of Electric Motor Design and Control Parameters Based on Ant Colonies Speed Trajectory Optimization

EvangelosM. Tsampouris, Panagiotis E. Kakosimos, and AntoniosG. Kladas

Department of Electrical and Computer Engineering National Technical University of Athens, Zografou 15780, Greece

The multiplicity of operational and technical specifications, characterizing the design of electric drives, favors the application of coupled computation techniques. When the combined optimization of steady-state and transient-state operation is required in terms of energy efficiency versus speed performance, the coupled computation of electric motor design and control parameters can be utilized. In this paper, a particular electric motor design technique is introduced, based on the simultaneous optimization of motor steady-state performances and speed controller transient responses. The proposed methodology has been applied for the optimization of a Permanent Magnet Synchronous Machine (PMSM) drive and offered practical reduction of the complex optimization criterion cost when compared to the decoupled approach. Implementation of the resulting drive system has been undertaken, and overall performance improvements have been experimentally validated.

Index Terms—Ant colony optimization, design optimization, energy efficiency, performance evaluation, permanent magnet machine.

I. Introduction

DESIGN and control of traction motors based on multi operating points performance and efficiency criteria is nowadays a common place. This has been the result of numerous contributions, on the enhancement both of the design and control methodologies, applicable to electric drives [1]. Despite the extensive diffusion of methodologies, little work has been done on the integration of these tools on a system-design suit [2]. Moreover, a coupled optimization of the overall system is yet to be addressed.

In this paper a novel design concept is introduced, for the coupled computation of design and control parameters of electric motors, based on the optimization of the motor speed transient response. Specifically, an ant colony optimization (ACO) routine has been developed for the computation of optimum motor speed trajectories, based on an integral drive system model. The latter has been coupled to a 0th order Rosenbrock-based motor design optimization routine, presented in previous work [3]. The algorithm offered improved convergence characteristics, when compared to the decoupled motor geometry and controller gain optimization. The resulting drive system configuration has been experimentally tested under several control input profiles and efficiency improvements have been experimentally validated.

II. System Layout and Operation

The optimization suit comprises of the motor geometry and the speed trajectory optimization modules (modules "A" and "B," respectively), as illustrated in Fig. 1 and (1).

At k-iteration, each module contributes to a subset of the objective function terms. For the evaluation of these terms, iterative calls to particular system models are generated by the optimization modules A and B. More specifically, module A iteratively calls the 2D FEM of the PMSM in order to compute its steady-state performance characteristics, through a two-step analysis, described in paragraph II.A. Module B respectively calls an integral Matlab/Simulink model of the vector controlled, Maximum Torque Per Ampere (MTPA) PMSM drive, in order to assess the dynamic performances of the motor, in terms of energy consumption versus speed response time (paragraph II.B). This has been achieved by interfacing an ACO routine with the drive system model that enabled the computation of optimum acceleration paths for each geometry under consideration.

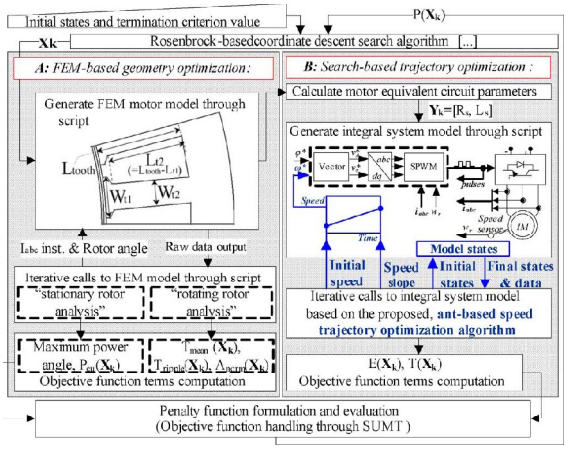

Fig. 1. Optimization system layout.

$$
\begin{aligned}
P^k(\mathbf{X_k}) = {} & G_1 \frac{T_{\text{mean}}(\mathbf{X_k})}{T_{\text{mean}}(\mathbf{X_0})} + G_2 \frac{T_{\text{ripple}}(\mathbf{X_k})}{T_{\text{ripple}}(\mathbf{X_0})} \\
& + G_3 A_{\text{norm}}(\mathbf{X_k}) \\
& + G_4 \frac{T_{\text{mean}}(\mathbf{X_k})}{\sqrt{P_{\text{cu}}(\mathbf{X_k})}} \left(\frac{T_{\text{mean}}(\mathrm{X_0})}{\sqrt{P_{\text{cu}}(\mathbf{X_0})}} \right)^{-1} \\
& + G_5 \frac{C(\mathbf{X_k})}{C(\mathbf{X_0})} \\
& + G_6 \frac{E(\mathbf{X_k})|_{(G_E E(\mathbf{X_k}) + G_T T(\mathbf{X_k}))_{\text{opt}}}}{E(\mathbf{X_0})} \\
& + G_7 \frac{T(\mathbf{X_k})|_{(G_E E(\mathbf{X_k}) + G_T T(\mathbf{X_k}))_{\text{opt}}}}{T(\mathbf{X_0})} \\
& + R^k \sum 1/(g_i(\mathbf{X_k})),\ R^k > 0 \qquad (1)
\end{aligned}
$$

Manuscript received November 09, 2012; revised January 11, 2013; accepted January 20, 2013. Date of current version May 07, 2013. Corresponding author: E. M. Tsampouris (e-mail: etsab@central.ntua.gr).

Color versions of one or more of the figures in this paper are available online at http://ieeexplore.ieee.org.

Digital Object Identifier 10.1109/TMAG.2013.2243909

where: $\mathbf{X_k} = [L^k_{\text{tooth}},\ W^k_{t1},\ W^k_{t2}]$ (see also Fig. 1)

G_1–G_7: weight coefficients $\in (0, 1)$

$T_{\text{mean}}, T_{\text{ripple}}$: mean, ripple torque (N*m)

P_{cu}: copper loss (W)

A_{norm}: 3rd and 5th h. EMF normalized amplitudes sum

$C(\boldsymbol{X_k})$: technical cost terms, modeling manufacturing cost variations with the winding fill factor and the slot shape respectively, of the form of (2), as described in [3].

$$\begin{aligned} C(\mathbf{X_k}) &= C_1\left(\frac{L^k_{\text{tooth}}}{L},\ \frac{W^k_{t2}}{W}\right) \\ &\quad + C_2\left(\frac{W^k_{t1}}{W^k_{t2}},\ \frac{W^k_{t2}}{L^k_{\text{tooth}}}\right) \\ &= \sum_{i=1}^{4}\sum_{j=1}^{3} a_{ij}\exp\left(-\left(\frac{(x_i - b_{ij})}{c_{ij}}\right)^2\right), \\ (L, W) &= \max(L_{\text{tooth}}, W_{t2}) \end{aligned} \tag{2}$$

$E(\mathbf{X_k})|_{(G_E E(\mathbf{X_k}) + G_T T(\mathbf{X_k}))_{\text{opt}}}$: Energy consumption (mWh)

$T(\mathbf{X_k})|_{(G_E E(\mathbf{X_k}) + G_T T(\mathbf{X_k}))_{\text{opt}}}$: System response time (sec), both calculated for 0%–100% acceleration, under 2nd order static load torque—speed characteristic, for the optimum acceleration path case (3).

G_E, G_T: gain coefficients (Wh^{-1}, sec^{-1}).

These model-based and search-based computations are finally used for the evaluation of the proposed penalty function formula, given in (1).

The proposed multiobjective function formula, is an expansion of the classical form, used for the optimization of steady-state motor performances [2]–[4]. The main concept of the proposed modification is to investigate the possibility of developing system level design strategies, in the case of high performance electric drives, in a way that expands the traditional multiobjective basis by including both steady state and transient state performance as well as technical cost criteria.

The novelty of this contribution relies on the constitution of the particular speed trajectory optimization module, based on ACO, which allows for a weighted estimation of the traction system dynamic performance during motor design, on the basis of energy consumption (E) versus response time (T).

TABLE I
MACHINE PROTOTYPE DESIGN CHARACTERISTICS (DIMENSIONS IN MM)

General	Number of phases	3
	Number of poles	28
	Motor active length	100
Rotor	Magnet inner radius	32.75
	Magnet (rotor) outer radius	35.75
	Magnet angle	9. 78 deg
Gap	Gap width	0.50
Stator	Stator outer radius	50

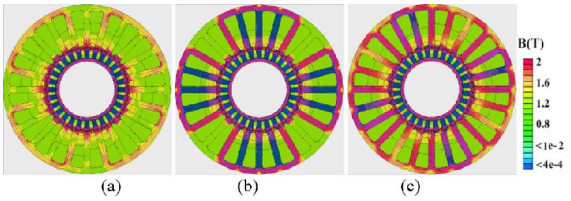

Fig. 2. FEM solution snapshots. (a)–(b) "stationary rotor analysis." (a) no load. (b) full load condition. (b)–(c) "rotating rotor analysis." (b) 0 deg. (c) 360/28/2 deg. rotor angular displacement.

The methodology has been applied to optimize a Fractional Slot single layer Concentrated Winding (FSCW) PMSM, with surface permanent magnet topology. In a first step, an estimation of the motor structure is achieved by considering classical machine design techniques. Table I summarizes the basic properties of the surface mounted PMSM prototype.

Parametric 2D FEM of the PMSM is then introduced, by utilizing convenient Matlab scripting.

A. FEM Based Geometry Optimization

At k-iteration, two sets of magnetostatic analyses, determine steady-state performances. During the "stationary rotor analysis," phase shifting of the stator currents occurs, enabling the calculation of maximum power angle and respective copper loss. This power angle is then kept constant through the next "rotating rotor analysis" stage, by synchronously rotating the rotor and stator MMFs. During this second set of analyses, all the steady state performance terms are calculated and sent to the penalty function evaluation module.

Fig. 2(a) and (b) shows FEM solution snapshots during the first iteration $(k = 1)$, in the case of the "stationary rotor analysis," involving different loading levels of the PMSM. These figures illustrate the circumferentially inhomogeneous magnetic field distribution created by the fractional slot windings in the machine, accentuating local saturation effects and nonlinear behavior with current. Fig. 2(b) and (c), respectively, present snapshots of the "rotating rotor analysis" for the same stator currents and different rotor angular displacements, corresponding to PMSM synchronous operation. These figures show the important impact on the flux distribution and saturation level in this type of machines of small internal angle variations. During each call the PMSM geometry is reconstructed and retriangulated through an external Matlab-Lua interface script. The respective FEMs contain, in average, 34500 nodes.

B. Search Based Trajectory Optimization

In order to additionally account for the dynamic performance of the PMSM, a combinative, energy consumption versus re-

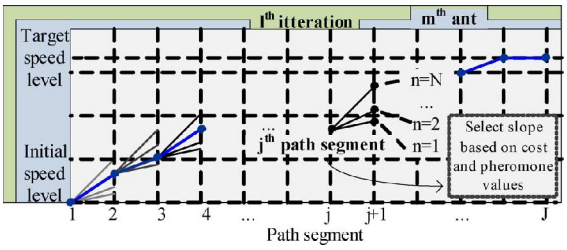

Fig. 3. Graphical explanation of the proposed ant colony speed trajectory optimization algorithm.

sponse time criterion has been introduced. The later is calculated under properly specified control input, so that comparable performances can be acquired.

For each design input vector $\mathbf{X_k}$ a corresponding vector of stator equivalent circuit parameter values, $\mathbf{Y_k} = [\mathrm{R_s},\ \mathrm{L_s}]$, is generated. ($\mathrm{R_s}$ and $\mathrm{L_s}$ is the phase resistance-inductance of the PMSM stator, calculated directly by the FEM script). A stochastic search process, based on ACO, in then applied on the resulting system model and the optimum acceleration path of the PMSM, satisfying (3), is computed.

$$(G_E E(\mathbf{X_k}) + G_T T(\mathbf{X_k}))_{\mathrm{opt}} = \min(G_E E^{\mathrm{path}}(\mathbf{X_k}) + G_T T^{\mathrm{path}}(\mathbf{X_k}))|_{\mathrm{path}=1,2,\ldots,\mathrm{PATH}}. \quad (3)$$

The proposed search algorithm methodology, integrated in the optimization module B of the developed system-level design suit, is graphically explained in Fig. 3.

As described in this figure, the proposed algorithm applies a stochastic search, over a quantized speed-time 2D space. At the jth-step of the mth-ant during lth-iteration, N input speed ramps, corresponding to N different speed slopes are simulated over a user defined time window (T_{sim}). For each one of the N simulations, energy consumption ($E(n, j, m, l)$) and estimated system response time ($T(n, j, m, l)$) are stored, along with the final states of the integral model. Results are then used to populate the cost matrix $[C_{\mathrm{dyn}}(\mathbf{X_k})] = G_E[E(\mathbf{X_k})] + G_T[T(\mathbf{X_k})]$. That is the model output matrix, which in combination with the pheromone matrix of the ACO algorithm is used in order to select the optimum jth-path segment, of the mth-ant during lth-iteration [5]. The procedure is then repeated, after updating the initial states of the Simulink model, until all the M ants have reached the target speed level or travelled for J path segments for the lth-time. In this stage, the best of the M paths (each one divided to a maximum of J segments) is selected and stored. The hole procedure is then restarted, for the $(l+1)$th iteration, after the ant pheromone is decayed and updated [5].

The algorithm stops when in a single iteration the standard deviation of path cost values ($1 \times M$ matrix) drops below 5%. The proposed termination criterion offers a convenient compromise between accuracy and computational cost, resulting to an average of 37 iterations for a complete run.

The proposed design of the ACO routine, enables the coupled computation of PMSM control and design parameters that affect motor dynamic performance, in terms of transient energy consumption versus transient response time. The optimum acceleration path of the drive is finally selected during the kth-iteration of the main Rosenbrock based search routine. Under this control input, the minimum dynamic performance cost (term$G_6(E(\mathbf{X_k})|_{(G_E E(\mathbf{X_k})+G_T T(\mathbf{X_k}))_{\mathrm{opt}}})/(E(\mathbf{X_0}))$ + $G_7(T(\mathbf{X_k})|_{(G_E E(\mathbf{X_k})+G_T T(\mathbf{X_k}))_{\mathrm{opt}}})/(T(\mathbf{X_0}))$ of (1)) is computed. The search for the optimum motor geometry is now guided from an updated penalty function formula, that expands the objectives of the optimization to a system-oriented, rather than a component-oriented level.

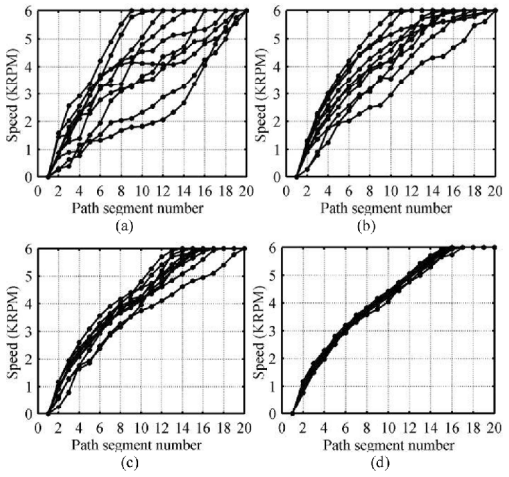

Fig. 4. Proposed ACO algorithm. (a) i = 10. (b) i = 20. (c) i = 30. (d) i = 40.

III. Results and Discussion

The methodology has been applied to optimize the FSCW PMSM of Fig. 2. Fig. 4 presents the calculated acceleration trajectories, during the 1st iteration of the main search routine ($k = 1$) for the run (i) 10, 20, 30 and 40 of the proposed speed trajectory optimization algorithm. In the case considered, 10 ants ($M = 10$) travel for a maximum of 20 path segments ($J = 20$) while choosing between 10 slopes of the speed ramp ($N = 10$). A 20 msec simulation interval (T_{sim}) per path segment has been selected. Factors G_E and G_T have been set to handle energy consumption and response time criteria with equal priorities, while the PMSM operates under the static load torque-speed characteristic of (4).

$$T = T_0 + T_2 w^2 = 0.1T_{\mathrm{nom}} + 0.9T_{\mathrm{nom}} w^2 \quad (4)$$

where w is the normalized mechanical speed of the PMSM.

Fig. 4 illustrates the convenient convergence characteristics of the proposed ACO. In all the cases considered, the algorithm has converged to the optimum path and required a maximum of 53 cycles ($L_{\max} = 53$). The resulting optimum path of Fig. 4(d) approaches a parabolic curve, due to the direct impact that load torque profile has on the selection mechanism. The proposed ACO resets during each call to the main Rosenbrock search routine, while contributing the cost terms E and T, linked to the dynamic motor performance.

The optimized output of the design suit is compared to the initial user input in Table II, in the case of unary weight coefficient gains ($G_1 = G_2 = \cdots = G_7 = 1$). Fig. 5 compares the optimized speed trajectories of the respective PMSM configurations. As can be observed, even the performed fine tuning on the stator optimization vector $\mathbf{X_k}$, have a considerable effect on motor equivalent circuit parameters vector ($\mathbf{Y_k}$) and consequently on the optimum acceleration path of the resulting MTPA vector controlled drive.

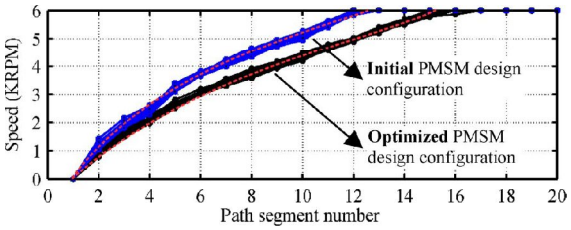

Fig. 5. Optimum acceleration paths of the PMSM drive.

TABLE II
OPTIMIZED PMSM DESIGN—EQUIVALENT CIRCUIT PARAMETER VALUES

Var.	Initial	Optimized	Change (%)
L_{tooth}(mm)	18.8	18.46	- 1.8
W_{t2} (mm)	4.6	4.74	3.04
W_{t1} (mm)	3.7	3.61	- 2.43
R_s (Ω)	0.401	0.395	-1.50
L_s (mH)	4.74	4.96	4.64

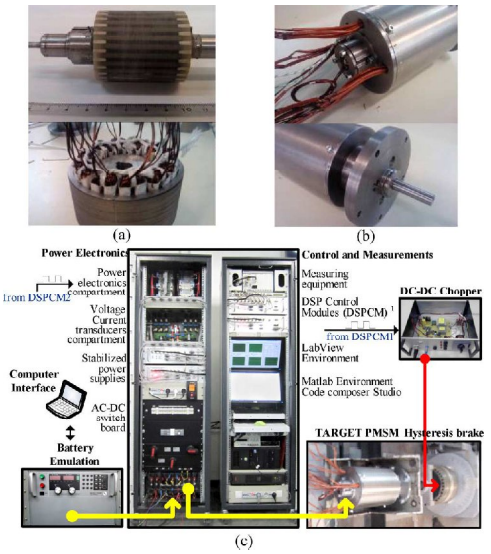

Fig. 6. Experimental validation. PMSM (a) rotor and stator (b) housing. (c) PMSM MTPA vector control drive and programmable load.

Such a phenomenon have to be addressed during the design of high performance PMSMs, destined for high load variability drives.

IV. EXPERIMENTAL VALIDATION

The optimized geometry has been introduced in a PMSM prototype [Fig. 6(a)–(b)], which has been integrated to the experimental test bench of Fig. 6(c). The later utilizes two Texas Instruments F2812 DSPs, along with data acquisition equipment implementing precise vector control of the PMSM under controllable speed-load torque input. The simulated optimum acceleration path of Fig. 5 as well as two detuned reference inputs are emulated. E and T terms are measured. Simulated and experimental results are compared in Table III. The good agreement of measured and simulated performances presented in Table III, under the speed input profiles of Fig. 7, validate the accuracy of the proposed modeling methodology.

Additionally, the experimental validation of the computed optimum acceleration performance confirms the suitability of the proposed ACO routine in the specific class of applications.

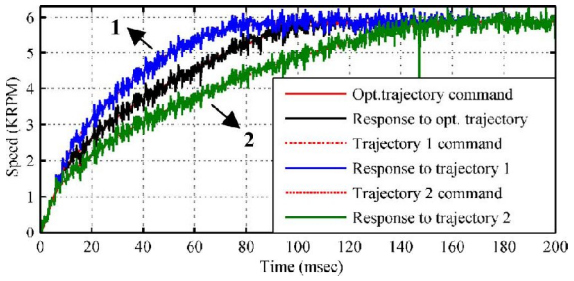

Fig. 7. Measured acceleration trajectories of the PMSM drive.

TABLE III
COMPARISON OF MEASURED AND SIMULATED E AND T VALUES

Trajectory	Simulated E(mWh) - T(msec) - $G_E E+G_T T$	Measured E(mWh) - T(sec) - $G_E E+G_T T$
1	52.7 - 74 - 1.93	54.3 - 74 - 2.03
2	34.4 - 140 - 1.87	36.1 - 142 - 1.94
Optimized	39.3 - 96 - 1.64	41.9 - 97 - 1.73

Finally, the practical importance of the methodology presented is validated by the measured variation of the complex optimization formula values under dynamic operation, $[C_{\mathrm{dyn}}(\mathbf{X_k})]$, with the motor speed response time. As can be observed by comparing Fig. 7 with Table III, a 20% change of the optimum speed response time, increases the overall dynamic performance cost of the drive system by a considerable 12%. As shown in Fig. 5, such a variation of the optimum response time can occur during motor design optimization, which also validates the practical importance of the proposed coupled computation.

V. CONCLUSION

A method for the coupled computation of electric motor design and control parameters, based on the ACO of the motor speed transient response was introduced. The later was applied to optimize an FSCW PMSM drive and provided system-oriented design capabilities combined with the experimentally verified method on the motor dynamic performance. The proposed ACO routine involves reduced memory space and execution time requirements, related to the dynamic operation cost of the drive system, when compared to the decoupled approach, while it can be easily implemented in a real-time, embedded speed controller.

ACKNOWLEDGMENT

This work was supported by the EU (European Social Fund—ESF) and Greek national funds through the Operational Program Synergasia under grant code 09SYN-51-988 entitled: Development of electric bus prototype.

REFERENCES

[1] A. M. El-Refaie, *IEEE Trans. Ind. Electron.*, vol. 57, no. 1, pp. 107–121, Jan. 2010.
[2] A. Sarikhani and O. A. Mohammed, *IEEE Trans. Magn.*, vol. 47, no. 5, pp. 1266–1269, May 2011.
[3] E. M. Tsampouris, M. E. Beniakar, and A. G. Kladas, *IEEE Trans. Magn.*, vol. 48, no. 2, pp. 943–946, Feb. 2012.
[4] K. Jeonghu, M. Seungjae, and H. Jung-Pyo, *IEEE Trans. Magn.*, vol. 46, no. 6, pp. 2108–2111, Jun. 2010.
[5] M. S. Kwang and H. S. Weng, *IEEE Trans. Syst., Man Cybern.*, vol. 33, no. 5, pp. 560–572, Sep. 2003.